Published in final edited form as:
Nat Chem Biol. 2014 January ; 10(1): 29–34. doi:10.1038/nchembio.1381.

Chemical inhibition of prometastatic lysyl-tRNA synthetase–laminin receptor interaction

Dae Gyu Kim[1,2,15], **Jin Young Lee**[1,2,15], **Nam Hoon Kwon**[1,2], **Pengfei Fang**[3], **Qian Zhang**[4], **Jing Wang**[3], **Nicolas L. Young**[5], **Min Guo**[3], **Hye Young Cho**[6], **AmeeqUl Mushtaq**[6], **Young Ho Jeon**[6], **Jin Woo Choi**[1,7], **Jung Min Han**[1,2], **Ho Woong Kang**[8], **Jae Eun Joo**[8], **Youn Hur**[8], **Wonyoung Kang**[9], **Heekyoung Yang**[9], **Do-Hyun Nam**[9], **Mi-Sook Lee**[2], **Jung Weon Lee**[2], **Eun-Sook Kim**[10], **Aree Moon**[10], **Kibom Kim**[1,2], **Doyeun Kim**[1,2], **Eun Joo Kang**[1], **Youngji Moon**[1], **Kyung Hee Rhee**[2], **Byung Woo Han**[2], **Jee Sun Yang**[11], **Gyoonhee Han**[11], **Won Suk Yang**[1,2], **Cheolju Lee**[12], **Ming-Wei Wang**[13], and **Sunghoon Kim**[1,2,14,*]

[1]Medicinal Bioconvergence Research Center, College of Pharmacy, Seoul National University, Seoul 151-742, Korea

[2]Research Institute of Pharmaceutical Sciences, College of Pharmacy, Seoul National University, Seoul 151-742, Korea

[3]Department of Cancer Biology, The Scripps Research Institute, Scripps Florida, Jupiter, FL 33458, USA

[4]Department of Chemistry and Biochemistry, Florida State University, Tallahassee, FL 32306, USA

[5]Ion Cyclotron Resonance Program, National High Magnetic Field Laboratory, Florida State University, Tallahassee, FL 32310, USA

[6]College of Pharmacy, Korea University, Sejong 339-700, Korea

[7]Wellman Center for Photomedicine, Massachusetts General Hospital, Harvard Medical School, Boston, MA 02114, USA

[8]Yuhan Research Institute, Yongin 446-902, Korea

[9]Department of Neurosurgery, Samsung Medical Center, Sungkyunkwan University School of Medicine, Gangnam-Gu, Seoul 135-710, Korea

[10]College of Pharmacy, Duksung Women's University, Seoul 132-714, Korea

[*]Corresponding Author: Tel: 82-2-880-8180, FAX:82-2-875-2621, sungkim@snu.ac.kr.
[15]These authors contributed equally to this work.

Competing financial interests
The authors declare no competing financial interests.

Author contributions
D.G.K., J.Y.L., S.K. designed experiments. D.G.K., J.Y.L., P.F., Q.Z., J.W., H.Y.C., A.U.M., J.W.C., H.W.K., J.E.J., W.K., H.Y., M.-S.L., E.-S.K., E.J.K., J.S.Y., W.S.Y., J.S.Y. performed experiments. D.G.K., J.Y.L., N.H.K., N.L.Y., M.G., Y.H.J., H.W.K., Y.H., D.-H.N., J.W.L., A.M., J.M.H., G.H., C.L., S.K. analyzed the data. Y.H., K.K., Y.G.M., D.K., K.H.R., B.W.H. provided materials and supported experiments. D.G.K., N.H.K, M.G., Y.H.J., Y.H., S.K. wrote the manuscript. D.G.K., J.Y.L., N.H.K., M.G., Y.H.J., H.W.K., Y.H., D.-H.N., S.K. reviewed the manuscript. D.G.K., J.Y.L., N.H.K., M.G. Y.H.J., G.H., M.W.W., K.M.-F., S.K. discussed the results and commented.

[11]Translational Research Center for Protein Function Control, Department of Biotechnology and WCU Department of Biomedical Sciences, Yonsei University, Seodaemun-gu, Seoul 120-749, Korea

[12]BRI, Korea Institute of Science and Technology, Seongbuk-gu, Seoul 136-791, Korea

[13]The National Center for Drug Screening, Zhangjiang High-Tech Park, Shanghai, China

[14]WCU Department of Molecular Medicine and Biopharmaceutical Sciences, Seoul National University, Seoul 151-742, Korea

Abstract

Lysyl-tRNA synthetase (KRS), a protein synthesis enzyme in the cytosol, relocates to the plasma membrane after a laminin signal and stabilizes a 67-kDa laminin receptor (67LR) that is implicated in cancer metastasis; however, its potential as an antimetastatic therapeutic target has not been explored. We found that the small compound BC-K-YH16899, which binds to KRS, impinged on interaction of KRS with 67LR and suppressed metastasis in 3 different mouse models. The compound inhibited KRS–67LR interaction in two ways. First, it directly blocked the association between KRS and 67LR. Second, it suppressed the dynamic movement of the N-terminal extension of KRS and reduced membrane localization of KRS. However, it did not affect the catalytic activity of KRS. Our results suggest that specific modulation of a cancer-related KRS–67LR interaction may offer a way to control metastasis while avoiding the toxicities associated with inhibition of the normal functions of KRS.

Because metastasis is the primary cause of death related to cancer[1], novel therapeutic targets to control metastasis are a hot topic of research. Invasion is the initiation step of cancer metastasis, and this step requires proteolytic degradation of surrounding tissues and the extracellular matrix (ECM) and a change in cancer cell adherence. The proteolysis of ECM paves the way for invasion, and the dynamic switch of interaction between cancer cells and ECM transmits signals for cell migration[1,2]. Laminin is a major constituent of ECM and plays critical roles in cell adhesion, differentiation, and migration[2]. Laminin induces a signal propagation pathway leading to the induction of matrix metalloproteinase 2 (MMP-2), which is involved in the degradation of ECM[3]. Laminin also activates phosphatidylinositol-3 kinase and p38 mitogen-activated protein kinase (MAPK)[4] and induces cell migration by interacting with receptors such as integrins and 67-kDa laminin receptor (67LR).

67LR has attracted much attention as a marker of metastasis in various cancers[2,4–10]. High expression levels of 67LR in breast, lung, ovary, colon, and prostate carcinomas and in lymphomas have been reported, and it is known to be positively correlated with cancer progression and malignancy[7,9,11,12]. 67LR stabilizes the interaction between laminin and cell surface integrins. This receptor also induces conformational changes in laminin when binding to it, and thereby stimulates proteolytic cleavage of laminin to promote tumor cell migration[2]. All these findings point to the importance of 67LR in cancer metastasis, making 67LR a promising target for antimetastatic therapeutics.

The 67LR protein is a dimeric form of 37-kDa laminin receptor precursor (37LRP), a ribosomal subunit protein in the cytosol[10]. The dimerization process of 67LR and its preferential localization in the plasma membrane are not well understood. It is simply known that fatty acylation is necessary for the conversion process[13]. The membrane stability of 67LR increases when it associates with lysyl-tRNA synthetase (KRS), which enhances cell migration[4]. Although 37LRP has the potential for interaction with KRS, KRS preferentially binds to and controls the stability of 67LR in the plasma membrane[4].

Human KRS is an enzyme essential for protein synthesis and normally resides within the multi-tRNA synthetase complex (MSC)[14] in the cytosol; however, it performs dynamic functions as a result of various stimuli, moving to the nucleus or the extracellular space[15,16]. After a laminin signal, p38 MAPK phosphorylates KRS at the T52 residue, and KRS translocates to the plasma membrane, where it protects 67LR from ubiquitin-mediated degradation[4]. In light of the role of 67LR as a metastasis marker, we hypothesized that KRS would promote metastasis via 67LR and that we could control metastasis by inhibiting the interaction between the two proteins. In this work, we investigated the pathological role of KRS in promoting metastasis *in vivo* and its potential as an antimetastatic therapeutic target.

RESULTS

KRS enhanced cancer metastasis

We, therefore, verified the effect of KRS on the invasive characteristics of cancer cells by investigating the following issues in squamous cell lung carcinoma H226 cells: (1) laminin-dependent localization of 67LR and KRS in the plasma membrane, (2) laminin-dependent interaction of KRS and 67LR detected using immunoprecipitation (IP), (3) effect of KRS on the level of membranous 67LR, and (4) KRS-dependent cell migration and invasion analyzed using Transwell chamber and Matrigel invasion assays, respectively (Supplementary Results, Supplementary Fig. 1a–e). These results demonstrated that KRS was localized in the plasma membrane and associated with 67LR upon laminin signaling, thereby enhancing the stability of 67LR. The increased stability of 67LR in KRS-overexpressing H226 cells significantly enhanced cell migration and invasion (about 3-fold).

We then evaluated the significance of KRS for metastasis *in vivo*. Because the highly metastatic 4T1 cells showed the same behavior as H226 cells with regard to the KRS-dependent 67LR stability and KRS–67LR interactions (Supplementary Fig. 2), we created two KRS-overexpressing stable 4T1 cell lines (KRS-1 and KRS-2; Supplementary Fig. 3a), and injected each of them subcutaneously into mice in order to analyze the effect of the KRS overexpression on metastasis to the lungs. We found that the upregulation of KRS significantly increased the pulmonary nodule count more than 2-fold (Fig. 1a, b) with little effect on the weight and volume of primary tumors (Supplementary Fig. 3b, c). Conversely, we repeated the same experiments using 4T1 cells stably expressing anti-KRS short hairpin RNA (shRNA), sh-KRS-1 and sh-KRS-2, to suppress KRS expression (Supplementary Fig. 3d). The two anti-KRS shRNA cell lines showed a reduction in the number of pulmonary nodules by approximately 85% (Fig. 1c, d). Again, we observed little or no effect on the weight or volume of primary tumors (Supplementary Fig. 3e, f).

To assess the effect of KRS-dependent 67LR stability on metastasis, we analyzed the amounts of KRS and 67LR in the primary tumor and in the pulmonary nodules using immunohistochemistry (IHC) and immunoblotting, respectively. The levels of 67LR were proportional to the expression level of KRS in primary tumors, while they did not show an apparent correlation with KRS levels in the metastatic nodules (Supplementary Fig. 4a–c). These findings suggest that the KRS–67LR interaction, especially in the primary tumor, was a critical factor for cancer metastasis.

Because integrins as well as 67LR mediate laminin signal transduction, we further investigated the type of laminin receptor that is required for the membrane localization of KRS. We reduced the expression level of integrins and 67LR by means of integrin β1-specific and 37LRP-specific siRNAs, respectively, and analyzed the amounts of membranous KRS and 67LR (Supplementary Fig. 5a, b). Downregulation of integrin β1 reduced the laminin-dependent relocation of KRS to the plasma membrane and reduced the level of 67LR, whereas a knockdown of 67LR did not affect the KRS level in the membrane. On the basis of these results and a previous study[4], we concluded that an integrin-mediated signal cascade activated KRS upon laminin stimuli, and the activated KRS regulated cell motility by controlling 67LR stability.

Hit identification and optimization

To determine whether we can control metastasis by inhibiting the interaction between KRS and LR, we set up an yeast two-hybrid (Y2H) assay where the interaction of the two proteins would support cell growth, and we screened synthetic compounds for inhibition of cell growth (Fig. 2a and Supplementary Table 1). Out of 2,988 compounds tested, 6 specifically inhibited the interaction of the two proteins without affecting other interacting pairs such as KRS–AIMP2[17] and MRS–AIMP3[18] that are also the components of MSC (Supplementary Fig. 6a, b). Among these 6 compounds, BC-K01 (**1**) (2-(2-{[4-(methyl)benzoyl]imino}benzothiazol-3-yl)butanoic acid) met all 5 of Lipinski's criteria (Fig. 2b and Supplementary Table 1). BC-K01 reduced the binding of the two proteins in pull-down and IP assays (Supplementary Fig. 6c, d) and decreased the level of 67LR in the plasma membrane in a concentration-dependent manner (Supplementary Fig. 6e). BC-K01 effectively inhibited the effect of KRS on cell migration[4] judging by a cell morphology change, actin rearrangement, and phosphorylation of focal adhesion kinase (FAK; Supplementary Fig. 7a). It also suppressed the activity of MMP-2, cell migration, and invasion (Supplementary Fig. 7b–d).

To improve its efficacy and metabolic stability *in vivo*, we synthesized 1,463 derivatives of BC-K01 and compared them with BC-K01 using the above-mentioned functional assays (Supplementary Fig. 8a). Among the derivatives, we selected 54 candidates based on their ability to specifically inhibit the binding of the KRS–LR pair and further compared their antimigratory activity and cytotoxicity (Supplementary Fig. 8a, b). From these two rounds of screening, we finally chose BC-K-YH16899 (YH16899) (**2**) (2-(5,6-difluoro-2-{[3-(trifluoromethyl)benzoyl]imino}benzo[d]thiazol-3(2H)-yl)butanoic acid; Fig. 2b and Supplementary Note) for further validation studies. YH16899 hindered the interaction between the two proteins according to *in vitro* pull-down (Supplementary Fig. 9a) and IP

(Fig. 2c) assays. As a result, YH16899 treatment decreased the amount of membranous 67LR, but not that of cytosolic 37LRP (Supplementary Fig. 9b). YH16899 also suppressed the induction of MMP-2 (Supplementary Fig. 9c), cell morphology change, actin rearrangement, FAK activation, and cell invasion judging by results of the above-mentioned functional assays (Fig. 2d, e). Because YH16899 consists of *R* and *S* enantiomers, we isolated each isoform and compared their inhibitory effects (Supplementary Fig. 10a–c). Both isoforms reduced the levels of membranous KRS and 67LR and suppressed cell invasiveness by approximately 80%, regardless of the type of isomerism. In summary, YH16899 showed a 3- to 6-fold improvement of IC_{50} compared to BC-K01 in most of the assays tested and exhibited better volume of distribution *in vivo* (Supplementary Table 2). Because KRS is essential for translation, we investigated the effect of YH16899 on the catalytic activity of KRS. YH16899 had little or no effect on the catalytic activity of KRS and cellular protein synthesis (Supplementary Fig. 11a–c), suggesting that the suppressive effect of YH16899 on cell migration did not result from reduced protein synthesis. To determine whether the effect of YH16899 is specific to cancer cells, we treated WI-26 and H226 cells with YH16899 and assessed cell viability and migration (Supplementary Fig. 12a, b). YH16899 did not affect the cell viability of the two types of cells, whereas it inhibited migration of cancer cells more significantly than that of normal cells. IC_{50} for inhibition of migration of WI-26 did not fall within the tested concentration range (0 to 50 μM), whereas the IC_{50} value for inhibition of H226 migration was 8.5 ± 2.1 μM (Supplementary Table 2). It is probably due to the relatively low expression of 67LR in WI-26 cells (Supplementary Fig. 12c), showing the specificity of YH16899 to the KRS–67LR expression as well as interaction. YH16899 was effective at suppressing cell migration and invasion of H226 (Fig. 2e, Supplementary Fig. 12b, and Supplementary Table 2), which expresses a high level of 67LR.

Comparative investigation of YH16899 versus direct blocking of 67LR showed that YH16899-mediated suppression of cell invasion (approximately 85%) worked as effective as siRNA treatment did (Supplementary Fig. 13). These data suggested that inhibition of the KRS-67LR interaction by YH16899 was sufficiently effective for suppression of the metastatic function of 67LR.

Next, we set up a chorioallantoic membrane (CAM) assay to analyze the intravasation of H226 cells. We injected H226 into CAM in the upper layer of embryos where blood vessels had already formed. During incubation, migratory H226 cells would spread through blood vessels after intravasation. We collected cells from the bottom region of chick embryos to isolate DNA and then performed quantitative PCR (qPCR) to detect the human *Alu* gene. On the basis of the detected amount of the human *Alu* gene, YH16899 inhibited H226 cell invasion by 80% compared to the control without chemical treatment (Fig. 2f).

YH16899 suppressed cancer metastasis *in vivo*

Using YH16899 as a lead compound, we examined how it would affect metastasis in three different *in vivo* models. First, we tested the efficacy of YH16899 in a mouse breast cancer model[19] whereby we injected 4T1 cells into a mammary fat pad. Oral administration of YH16899 at two different doses (100 and 300 mg/kg) inhibited tumor metastases to the

lungs by approximately 60% with little or no effect on body weight (Supplementary Fig. 14a–c). Because the lower dose yielded a robust suppressive effect, we used 100 mg/kg for further *in vivo* experiments.

The Tg(MMTV-PyVT) mouse is a well-known metastasis model that naturally develops primary breast tumors that spread to the lungs[20]. Tg(MMTV-PyVT) mice showed enhanced expression of KRS and 67LR (Supplementary Fig. 14d), suggesting that they can serve as a good model for the studies of KRS-mediated metastasis. We found that in this model, YH16899 also reduced pulmonary nodule formation by approximately 70% without affecting body weight (Supplementary Fig. 14e–g).

To test another metastasis model[21], we injected invasive A549 cells, expressing red fluorescent protein (RFP), into the left ventricle of the heart and monitored cancer cell colonization using *in vivo* photon imaging. The A549-RFP cells injected into the control group generated tumors in the brain and bones, but oral administration of YH16899 considerably reduced these metastases (Supplementary Fig. 14h). We monitored the suppressive effect of YH16899 using photon imaging for up to 7 weeks and found that YH16899 reduced the average radiance in the treated group by approximately 50% (Supplementary Fig. 14i). YH16899 also greatly enhanced survival in the treated group (Supplementary Fig. 14j). As described above, YH16899 did not affect the body weight (Supplementary Fig. 14k).

Additional analysis of hematological metrics and blood chemistry in ICR mice treated with high doses of the compound confirmed that YH16899 caused few side effects in mice (Supplementary Table 3). Taken together, these results suggest that chemical inhibition of the KRS–67LR interaction can suppress metastasis *in vivo* without severe toxicity.

YH16899 directly inhibited the KRS–67LR interaction

Human KRS comprises an N-terminal extension (N-ext, 1–72), an anticodon-binding domain (ABD, 73–209), and a catalytic domain (CD, 220–597; Fig. 3a). To determine the binding site of YH16899, we conducted surface plasmon resonance (SPR) analysis of YH16899 with the polypeptides $KRS_{1–597}$, $KRS_{1–207}$, and $KRS_{220–597}$. We observed preferential binding of the compound to the N-terminal domain, $KRS_{1–207}$ (Supplementary Figure 15a–e), which is known to interact with LR[4] (Fig. 3a). YH16899 did not show significant binding to 37LRP (Supplementary Figure 15d, e), suggesting that KRS is the main target of YH16899.

We then conducted nuclear magnetic resonance (NMR)–based chemical shift perturbation (CSP) analysis using the purified peptide $KRS_{1–207}$ in the presence of YH16899 to identify the residues that may be in proximity to YH16899. The addition of YH16899 strongly perturbed the G118, H120, G194, and E195 residues, and less strongly Y163, K164, and T191 (Supplementary Fig. 16a). We mapped these residues on the KRS structure in relation to the modeled docking of tRNA (Fig. 3b), and their localization is shown on the surface around the hydrophobic pocket formed by two loops and a β-sheet of ABD (Supplementary Fig. 16b). We compared the CSP data in the presence of a YH16899 racemic mixture, *S*, or *R* isomer with respect to the G118 and H120 residues at the binding site of $KRS_{1–207}$

(Supplementary Fig. 16c, d). As shown in the invasion assay and in 67LR stability analysis (Supplementary Fig. 10a–c), the affinities of the two enantiomers were not significantly different from each other, although the *S* enantiomer showed a slightly larger extent of NMR chemical shift changes. We performed a docking study of the two racemic forms (*R* and *S*) of YH16899 with the ABD and found that the most frequent docking positions consistent with the CSP data house the compound within the cavity surrounded by the perturbed residues (Fig. 3c). The original hit compound BC-K01 also showed a CSP pattern similar to that of YH16899 (Supplementary Fig. 17a, b), suggesting that the two compounds bind to ABD in a similar manner.

In these positions, the aromatic rings of YH16899 would likely be accommodated in the hydrophobic pocket formed by the side chains of L142, F144, M157, T191, and I199. This apolar pocket is further curved by the polar side chains of H120, N159, R161, and K192, thus forming a site optimal for protein binding and drug targeting[22,23]. To validate this binding model, we generated a series of alanine substitution mutants at the residues that may contact YH16899, and compared them in different functional assays as described above. The L142A and F144A mutants showed a strikingly reduced ability to bind YH16899, to inhibit KRS-LR interaction, to stabilize the membrane content of 67LR, and to promote cell invasion (Fig. 3d and Supplementary Fig. 18a–f). These results support the docking site of YH16899 in the ABD, and further show that YH16899 and 67LR share at least some residues involved in binding to KRS. Importantly, none of these KRS mutations influenced the aminoacylation activity of KRS, protein synthesis, or cell viability (Supplementary Fig. 18g–i). On the basis of these results, we propose that YH16899 directly interferes with the association of 67LR with KRS via competitive binding to critical residues but does not affect the catalytic activity of KRS.

YH16899 suppressed membrane translocation of KRS

Because KRS is normally bound to MSC in the cytosol, it must be released from the complex in order to relocate to the plasma membrane. We thus set out to determine whether YH16899 can also affect the association of KRS with MSC as well as the plasma membrane localization of KRS. Under physiological conditions, KRS requires phosphorylation at T52 (p-T52) to be released from MSC in the cytosol[4]. We analyzed the structure of p-T52 KRS using the T52D mutant, a mimetic of the p-T52 form, by means of small-angle X-ray scattering (SAXS) and hydrogen/deuterium exchange mass spectrometry (HDX-MS). Compared with the WT KRS, the T52D mutant showed a more extended solution envelope and an increased deuterium exchange rate (Fig. 4a, Supplementary Table 4, and Supplementary Fig. 19a–c). The model of the KRS T52D mutant suggested that phosphorylation at T52 could open up the ABD-CD interface and disturb the binding pocket for AIMP2, the binding partner of KRS within MSC[14,24], thereby releasing p-T52 KRS from MSC (Fig. 4a and Supplementary Fig. 19b, c). To confirm this prediction, we set up an *in vitro* assay to quantify the interaction between KRS and AIMP2 and compare the binding of KRS WT and the T52D mutant with AIMP2. The T52D mutant showed 4.6-fold weaker affinity for AIMP2 (with K_D of 333 nM) than KRS WT did (Supplementary Fig. 20a). Using this assay system, we also examined whether YH16899 affects KRS binding to AIMP2, and observed little or no change in the binding affinity after introduction of

YH16899, suggesting that YH16899 activity was specific to the KRS–67LR interaction (Supplementary Fig. 20b).

To determine whether YH16899 affects the conformation of KRS upon binding, we compared the SAXS solution envelopes of free and YH16899-bound KRS T52D forms. We found that incubating KRS T52D with YH16899 induced a conformational change. Particularly, N-ext folded back toward the body of KRS, reducing the overall length of KRS T52D by 30 Å (Fig. 4a and Supplementary Fig. 21). In addition, YH16899 dramatically reduced deuterium exchange in the N-domain (Fig. 4b and Supplementary Fig. 22), suggesting that it suppresses the dynamic movement of N-ext. Specifically, the A6, A34, A53, T52, and T56 residues in N-ext also showed chemical perturbation after the addition of YH16899 (Supplementary Fig. 16a), implying that N-ext can also interact with YH16899, although the signals were not strong. Interestingly, the chemical treatment significantly reduced membrane localization of KRS (Supplementary Fig. 18d), suggesting that the flexible N-ext might be necessary for the membrane penetration of KRS.

We also conducted an NMR binding study of N-ext with a phospholipid nanodisc and found that several backbone NMR signals were selectively perturbed by the addition of the phospholipid nanodisc. This observation further supports the notion that N-ext interacts with cellular membranes (Fig. 4c). We also observed that Myc–$KRS_{41–597}$ (ΔN), where 40 N-terminal residues of N-ext were deleted, did not localize to the plasma membrane (Supplementary Fig. 23). Interestingly, T52, A53, and T56, which were among the strongly perturbed residues upon addition of the phospholipid nanodisc, overlapped with those of the CSP experiments with YH16899 (Supplementary Fig. 16a). These experiments suggest that the membrane anchoring of KRS requires N-ext and that YH16899 can hinder the N-ext–mediated membrane localization of KRS. According to these results, YH16899 appears to inhibit the prometastatic association of KRS with 67LR in two ways. First, it binds to the residues that are critical for the interaction with 67LR, thereby directly blocking the interaction of the two proteins. Second, it suppresses membrane localization of KRS by restraining the flexible N-ext (Fig. 5).

DISCUSSION

Earlier studies reported that blocking or suppressing 67LR with specific antibodies or siRNAs reduces invasion of metastatic cancers[25,26]. Nonetheless, targeting 67LR or its precursor 37LRP may also hamper the normal functions of 67LR. The results of the current study suggest that specifically inhibiting the metastasis-promoting interaction of KRS with 67LR is an alternative way to reduce metastasis while allowing normal functions of 67LR to proceed unimpeded. In this regard, it is worth noting that high levels of KRS frequently occur in various cancers[16,27,28].

For a long time, aminoacyl-tRNA synthetases (ARSs) have been attractive targets for the development of antibiotics[29,30]. Recently, some progress was achieved in targeting the mammalian ARS for the treatment of human diseases. Febrifugine derivatives, including halofuginone, target prolyl-tRNA synthetase, and many laboratories study them in connection with the possibility of treatment of cancer, fibrosis, and inflammatory

diseases[31,32]. Threonyl-tRNA synthetase was identified as a target protein of anti-angiogenic borrelidin[33], and a peptide fragment derived from tryptophanyl-tRNA synthetase is gaining interest as a possible anti-angiogenic agent[34]. Cyclic peptides inhibiting the interaction between human immunodeficiency virus (HIV) type 1 capsid protein and KRS are also being developed to treat HIV infection[35]. All these approaches are indicative of the potential of human ARSs as novel therapeutic targets and agents of human diseases. From this perspective, targeting the KRS–67LR interaction has several benefits. First, it can control the prometastatic interaction between KRS and 67LR without affecting other activities of these two proteins. Second, targeting the KRS–67LR interaction is effective at inhibiting cancer cell invasion to the same extent as direct 67LR downregulation, according to the present study. In contrast to targeting the LR-binding activity of KRS, knocking down of LR expression adversely affects translation and cell viability[5,36]. We presumed that the effect of LR-specific siRNA on invasion was partially due to the impeded protein synthesis and cell growth. Given that YH16899 did not inhibit the catalytic activity of KRS, protein synthesis, and cell viability, YH16899 could be considered a specific metastasis inhibitor that causes few side effects in normal cells, which have relatively low levels of KRS and 67LR. Since 67LR is a well-known marker of cancer metastasis, targeting 67LR with antibodies or siRNA can be another option to treat metastasis. Antibodies against 67LR, however, may hamper other physiological functions of 67LR by blocking its interactions with its many partners. Again, suppression of 67LR with specific siRNA, apart from the delivery issue, would block not only membranous but also cytosolic activities, and this crude approach may produce various undesirable effects. Targeting the KRS–67LR interaction, therefore, may have advantages over direct inhibition of 67LR, especially from the standpoint of therapeutic specificity.

KRS is functionally versatile[4,15,16,37] and undergoes dynamic conformational changes for each of its distinct activities[15] (Fig. 5). Here we show that YH16899 can specifically block the membrane function of KRS with little influence on the catalytic activity of KRS, suggesting that it is feasible to target only one of its activities without affecting its other functions. Our work not only demonstrates that the membrane form of KRS is an effective target for controlling metastasis but also suggests that specific modulation of a pathology-related protein–protein interaction is a promising approach to the development of novel therapeutics.

ONLINE METHODS

Cell culture and materials

H226 and 4T1 cells were purchased from American Type Culture Collection. DMEM containing 10% (v/v) fetal bovine serum (FBS) and 1% (v/v) penicillin/streptomycin was used for culture of cell lines. Cells were incubated with laminin (10 μg/ml) for 1 h in a serum-free medium and subjected to immunoblotting. Cells were treated with compounds (4 h and 24 h for immunoblotting and 3-[4,5-dimethylthiazol-2-yl]-2,5-diphenyltetrazolium bromide [MTT] assay, respectively) in a serum-free medium after 1-h preincubation with laminin. Cytosolic and membranous fractions were separated using a ProteoExtract kit (Calbiochem). The shRNA against murine KRS and siRNAs targeting human KRS were

purchased from Sigma and Invitrogen, respectively. The sequences of shRNA and siRNA are shown below: sh-KRS, CCGGCGGCGAATCAACATGGTAGAACTCGAGTTCTACCATGTTGATTCGCCGTTTTTG; si-KRS, GCUGUUUGUCAUGAAGAAAGAGAUA.

Generation of stable cell lines

4T1 cells were transfected with Myc-tagged KRS-expressing pCDNA3 (Invitrogen) and KRS-specific shRNA-expressing pLKO.1 (puromycin) and were selected with G418 and puromycin, respectively. After 2 to 3 weeks, the clones were picked and checked for expression of KRS using Western blotting.

Cell migration and invasion assays

The cell migration assay was performed using 24-well Transwell chambers with polycarbonate membranes (8.0-μm pore size, Costar). H226 cells (1×10^5/well) were added to the top chamber coated with laminin (10 μg/ml). H226 cells were allowed to migrate for 12 h in the presence of a compound. For the cell invasion assay, Matrigel (1 mg/ml) in the serum-free cold cell culture medium was placed in the upper chamber of 24-well Transwell chambers with polycarbonate membranes and incubated at 37°C for 4 h for solidification. H226 cells were seeded in the upper chamber and the lower chamber was filled with the medium containing laminin (10 μg/ml). H226 cells were incubated with the compounds for 24 h. Cells attached to the membranes from migration and invasion assays were fixed with 70% methyl alcohol in PBS for 30 min, washed with PBS 3 times, stained with hematoxylin (Sigma-Aldrich) for 10 min, and washed with distilled water. After removal of nonmigrant cells from the top face of the membrane with a cotton swab, the migrant cells (those attached to the bottom side of the membrane) were counted in 3 randomly selected visual fields (magnification ×20) under a microscope.

Metastasis of stable 4T1 cells in mice

Mouse breast cancer 4T1 cells stably overexpressing murine KRS or murine KRS-specific shRNA were created. Several colonies were harvested and the expression level of KRS was analyzed using immunoblotting. Among them, two KRS-overexpressing cell lines (KRS-1 and KRS-2) and two KRS-knockdown cell lines (sh-KRS-1 and sh-KRS-2) were injected into the back of 6-week-old female BALB/cAnCr mice. Mice were sacrificed 30 days and 25 days after the inoculation with KRS-1/2 and sh-KRS-1/2, respectively, and the metastatic nodules in the lungs whose size was over 1 mm in diameter were counted after fixation of excised lungs in 10% (v/v) formalin for 24 h. The size and weight of primary tumors were also measured after the mice were sacrificed. Animal experiments were in compliance with the University Animal Care and Use Committee guidelines at Seoul National University.

Screening of compounds using the Y2H assay

The screening of compounds was performed based on the Y2H system to identify specific inhibitors of the KRS–LR interaction. LexA–KRS and B42–LR were co-introduced into yeast EGY/SH cells, which were then seeded in a 96-well plate containing 200 μl of a galactose medium without Ura, His, Trp, and Leu. Each compound (Comgenex library and

Yuhan synthetic compounds) was added into each well (final concentration of 50 μg/ml), and OD values were measured at 540 nm after 6-day incubation. Compounds inhibiting the growth of yeast more than 50% compared to the control were chosen. The selected compounds were further tested for their effect on the interaction of protein pairs in MSC such as LexA–KRS/B42–LR, LexA–KRS/B42–AIMP2, and LexA–MRS/B42–AIMP3 to find a specific activity interfering with KRS–LR.

CAM assay

An *in vivo* invasion assay using chick embryos was performed as previously described[38] with some modifications. H226 cells resuspended in PBS (5×10^5) were mixed with YH16899 (50 μM), injected into a CAM of 9-day-old chick embryos and allowed to invade for 48 h. Genomic DNA was extracted from the lower part of the CAM, as described previously[39]. Primers and the probe specific for the human *Alu* sequence (sense, TCACGCCATTCTCCTGCCTCA; antisense, TCACGCCTGTAATCCCAGCACTTT; probe, 56-FAM/TCAGGAGAT/Zen/CGAGACCATCCCGGCTAAA/3IABkFQ) were used to amplify the human *Alu* repeats from the genomic DNA using qPCR. Chick *GAPDH* detected with specific primers (sense, TCTCTGGCAAAGTCCAAGTG; antisense, TCACAAGTTTCCCGTTCTCAG; probe, 56-FAM/AGTGCCCTT/Zen/GAAGTGTCCGTGT/3IABkFQ) was used as a control.

Metastasis of 4T1 cells from breast tumors in mice

For the 4T1 breast tumor metastasis experiment, 4T1 cells (4×10^4) were injected into the surgically exposed No. 2 mammary fat pad of anesthetized 7-week-old female BALB/cAnCr mice. Primary tumors were excised in 10 days after the inoculation (primary tumor volume: 100–150 mm^3), and the mice were divided into control and YH16899 treatment groups (dose: 100 or 300 mg/kg) with uniform distribution of resected primary tumor weights ($n = 5$ per group). The indicated concentration of YH16899 and methyl cellulose (MC, 0.5% v/v) was administered orally, once a day, starting on Day 1 after tumor resection. All mice were sacrificed and the lungs were excised at 28 days after the injection of 4T1 cells. Lungs were fixed in Bouin's solution, and pulmonary nodules were counted to assess metastases. All animals were maintained in accordance with the Yuhan Research Institute's Animal Care and Use Committee guidelines, with approved animal study protocols.

Metastasis of A549-RFP cells in mice

For the metastasis experiment with A549 cells, stable A549-RFP cells (1×10^6) were injected into the left ventricle of anesthetized 6-week-old female BALB/cAnCr nude mice ($n = 10$ per group). YH16899 (100 mg/kg) or MC solution (0.5% v/v) was administered orally once a day, starting on Day 1 after the inoculation for 130 days. An RFP photon signal of 5 randomly selected mice was detected using IVIS optical imaging every week from Week 4 to Week 7. Body weights were checked 2 times per week for 50 days and survival was followed up to the experimental end point (130 days). All animals were maintained in accordance with the Samsung Biomedical Research Institute's Animal Care and Use Committee guidelines, with approved animal study protocols.

Breast cancer metastasis in Tg(MMTV-PyVT) mice

Female FVB/N-Tg(MMTV-PyVT)6_{34}Mul/J transgenic mice (6 weeks old) were intraperitoneally injected with 100 mg/kg of YH16899 every other day for 6 weeks. The body weight was checked every 4 days for 6 weeks. Mice were sacrificed and lungs were excised and fixed with 10% (v/v) formalin for 24 h. The metastatic nodules on lungs were counted as described above. Animal experiments were in compliance with the University Animal Care and Use Committee guidelines at Seoul National University.

Total protein synthesis

H226 cells were treated with YH16899 at the indicated concentrations (Supplementary Fig. 11b, c). The cells were incubated with a methionine (Met)-free medium for 30 min, and [^{35}S]Met (10 mCi/ml) was added followed by incubation for 2 h. The cells were incubated again for 4 h in a complete medium and harvested. The harvested cells were lysed and the radioactivity was determined using scintillation counting. A lysine (Lys) incorporation assay was also performed as described above using a Lys-free medium and [^{3}H]Lys instead of a Met-free medium and [^{35}S]Met, respectively.

The MTT assay

Cells (1×10^4) were seeded in 96-well plates and treated with the compounds for 24 h. An MTT stock solution (5 mg/ml) was diluted 10-fold, and 10 μl of the diluted solution was added to each well containing 200 μl the medium and incubated for 30 min. The precipitated crystals were dissolved in 100 μl of DMSO. Absorbance was measured at 420 nm using a microplate reader (Sunrise, TECAN).

IP, FAK assay, zymography, and *in vitro* pull-down assay

H226 cells transfected with Myc-KRS were pretreated with 10 μg/ml laminin for 1 h in the serum-free medium and further incubated with compounds for 4 h. The cells were lysed and proteins were isolated from the lysate or membranous and cytosolic fractions for the IP and immunoblotting. For the zymography assay, H226 cells were treated with laminin (10 μg/ml) and compounds for 12 h. Proteins from the cell culture media were harvested and loaded onto a 10% SDS-PAGE gel containing 1 mg/ml gelatin. After SDS-PAGE, the gel was incubated in the reaction buffer and the gelatin-digested area around MMP-2 was visualized by staining with Coomassie Blue R250. For the *in vitro* pull-down assay, 37LRP was radioactively labeled using the TnT quick coupled transcription/translation system (Promega) and mixed with glutathione S-transferase (GST)–KRS (1 μg) in the presence of the indicated concentrations of compounds (Supplementary Fig. 9a). GST–KRS was pulled down and the coprecipitated 37LRP was detected using autoradiography. For FAK and actin analysis using immunofluorescence, H226 cells transfected with KRS were seeded in laminin-coated culture dishes and treated with a compound (50 μM). All other procedures have been described elsewhere[4].

SPR

The equilibrium dissociation constants of YH16899 with the His-tagged KRS WT, N-domain ($KRS_{1–207}$), and C-domain ($KRS_{220–597}$) were determined using BIAcore T-100

(GE Healthcare). GST-tagged 37LRP, KRS WT, and KRS point mutants were also purified for the SPR analysis. Each protein was diluted and adjusted to 30 μg/ml in 10 mM sodium acetate buffer (pH 5.0). Each protein was then applied to the surface of a CM5 Sensor Chip (GE Healthcare). YH16899 was diluted in PBS with 0.05% (v/v) Tween 20 and 2% (v/v) DMSO and injected at a flow rate of 20 μl/min at 25°C and the binding was determined by the change in resonance units (RU). For GST-tagged proteins, RU from the sensorgram of YH16899 binding to GST was deducted, and the apparent binding constant was obtained using 1:1 binding with a drifting baseline using the BIAevaluation program.

Composition of nanodiscs

DMPC (1,2-dimyristoyl-*sn*-glycero-3-phosphocholine) was solubilized in sodium cholate (Cholate:DMPC molar ratio 2:1) in a glass vial with a teflon-lined screw cap. The apolipoprotein MSP1D1 (Δ1–11 truncated membrane scaffolding protein) in buffer 10 mM Tris-HCl (pH 7.4), 100 mM NaCl, was mixed with the DMPC/Cholate solution and incubated for 2 h at 27°C with shaking at 150 rpm[40]. The optimal composition of nanodiscs was achieved with the molar ratio of MSP1D1:DMPC:Cholate at 1:40:80. Incorporation of the nanodiscs was initiated with addition of 80% w/v Biobeads SM2 (BioRad) for 2 h at 27°C with shaking at 150 rpm. Size exclusion chromatography of DMPC nanodiscs was carried out at a flow rate of 0.5 ml/min on a Superdex 200 16/60 GL gel filtration column (GE Healthcare) equilibrated with buffer 20 mM Tris-HCl (pH 7.4), 100 mM NaCl[40].

NMR analysis

Two N-terminal fragments of KRS, ^{15}N-labeled $KRS_{1–72}$ and $KRS_{1–207}$, were overexpressed and purified from *Escherichia coli* (*E. coli*), strain BL21(DE3), in M9 minimal medium enriched with $^{15}NH_4Cl$ as the sole nitrogen source (99% ^{15}N; Cambridge Isotope Laboratories). NMR titration experiments of YH16899 and BC-K01 were performed with 0.2 mM ^{15}N-labeled $KRS_{1–207}$ in buffer 20 mM HEPES (pH 7.0), 100 mM NaCl, 1 mM DTT. In the titration experiment, YH16899 or BC-K01 was added to the protein solution serially to the final concentrations of 0.2, 0.4, and 0.8 mM, and the ^{1}H-^{15}N TROSY experiments were monitored at 298 K. Similarly, for the titration of phospholipid nanodiscs with DMPC/DHPC (1,2-dicaproyl-*sn*-glycero-3-phosphocholine), the nanodisc was added to the 0.2 mM $KRS_{1–72}$ solution to final concentrations of 0.1 and 0.2 mM. The backbone assignment of ^{13}C,^{15}N-labeled $KRS_{1–72}$ and $KRS_{1–207}$ was performed with series of triple-resonance 2D and 3D experiments. Data were processed with NMRpipe[41] and analyzed with CCPN2.1.5[42]. CSP of ^{15}N and ^{1}H nuclei were analyzed by overlaying the ^{1}H-^{15}N TROSY spectra of free protein with those with YH16899 in a different molar ratio. The magnitude of the combined ^{1}H-^{15}N chemical shift differences (Δδ, ppm) was calculated using the equation $\Delta\delta=\{(\delta H^2)+0.2\times(\delta N^2)\}^{1/2}$, where δH and δN are changes to the proton (^{1}H) and nitrogen (^{15}N) chemical shifts, respectively[43]. All NMR spectra were recorded using an Avance 600 MHz NMR spectrometer equipped with a triple-resonance probe (Bruker).

Molecular docking analysis

AutoDock 4.2[12] software was employed to conduct the docking calculations. Structure of KRS ABD (pdb3bju) was prepared and Gasteiger charges were assigned. A YH16899-

binding site was determined from CSP-mapped residues obtained from the NMR titration experiments and the center of the grid box was set to the center of a binding-site cavity with grid dimensions at 28 × 24 × 32 $Å^3$ and 0.458-Å grid spacing. Protein structure was kept rigid in docking. Stereo isomers *R*- and *S*- of YH16899 were modeled with SYBYL-X 2.0 molecular modeling package (http://tripos.com), and energy was minimized with Gasteiger-Hückel charge set in a vacuum dielectric environment, using Powell algorithm and Tripos force field for 5,000 iterations subject to a termination gradient of 0.05 kcal/(mol·Å). The docking calculations were performed using the Lamarckian genetic algorithm and a population size of 150, and 2.5 million energy evaluations were used for 100× searches. The AutoDock calculations were performed on a Linux workstation with an Intel Xeon 2.93 GHz Quad core processor. A representative docking pose was selected from the most populated cluster. PyMOL (http://www.pymol.org) was used for manual inspection of interactions.

SAXS data collection and analysis

The human full-length *KRS* gene (corresponds to a 597-aa protein) was previously codon-optimized and cloned in the vector pBADito (Invitrogen, Grand Island, NY) with a C-terminal His 6×-tag[14]. Human KRS WT, S207D, and T52D mutants were expressed in the bacterial strain *E. coli* BL21(DE3), and purified to homogeneity using a Ni-HiTrap affinity column (5 ml) and a gel filtration Superdex 200 column (10/300 GL, GE Healthcare). All SAXS data were collected at the SIBYLS beamline at electron energy of 12 keV covering the $0.011 < S < 0.35$ $Å^{-1}$ range of momentum transfer[29,44]. Buffer exchange for WT and mutant KRS was performed using gel filtration. Proteins were loaded at concentrations of 15–20 mg/ml, and only the peak fraction of each protein sample was used without further concentration. In addition, T52D was also incubated with 1 mM YH16899 or DMSO at 22°C as a control. All samples were isolated one day prior to data collection, flash-frozen with liquid nitrogen immediately after elution from gel filtration and stored frozen. SAXS data were collected for 3 serial dilutions of each sample at a maximum of 6 and a minimum of 1 mg/ml. Data were collected from 2 short exposures (0.5 s) and one long exposure (6 s) for each protein sample at room temperature (18–21°C). Data scaling, merging, and evaluating were carried out by means of PRIMUS[45]. GNOM was used to evaluate the P(r) function[46]. The value of the maximum diameter of the particle, D_{max}, was determined empirically by examining the quality of the fit to the experimental data for a range of D_{max} values. *Ab initio* free atom modeling was performed using the DAMMIF program with the scattering curves as the fitting target[47]. Forty independent simulations were performed for each sample. Superposition, averaging, and filtering with the DAMAVER program yielded shape reconstructions[45]. These envelopes were then used as a guide to fit the crystal structures by rigid body modeling with PyMOL and Chimera[31].

For the spatial arrangement of the chemically perturbed residues on KRS with tRNA, N-ext of human KRS was modeled on the SAXS envelope of KRS WT. The tRNAs were docked by superimposition of the human KRS structure (pdb3bju) with the yeast aspartyl-tRNA synthetase–$tRNA^{Asp}$ complex structure (pdb1asy).

HDX FT-ICR mass spectrometry

The HDX methods have been described previously[48,49]. HDX samples were prepared in the same way as those for the SAXS analysis. Briefly, 5 μl of a sample (20 μM) was mixed with 45 μl of 20 mM HEPES, pH 7.5, and 150 mM NaCl in D_2O to initiate each HDX reaction. HDX incubation periods were 0.5, 1, 2, 4, 8, 15, 30, 60, 120, and 240 min, each followed by simultaneous quench and proteolysis[50]. HDX was quenched by 1:1 (v/v) addition of protease type XIII solution in 1.0% formic acid to reduce the pH to ~2.3 and to initiate the 2-min proteolysis. The digested peptide fragments were separated by a fast LC gradient on a ProZap C_{18} column (Grace Davison, 1.5 m, 500 Å, 2.1 × 10 mm) to minimize back exchange[49]. A postcolumn splitter reduced the LC eluent flow rate to ~400–500 nl/min for efficient microelectrospray ionization (micro-ESI). Microelectrosprayed HDX samples were directed to a custom-built hybrid linear quadrupole ion trap 14.5 tesla FT-ICR (Fourier transform ion cyclotron resonance) mass spectrometer[51] (Thermo Fisher). The total data acquisition period for each sample was 6 min. Each experiment was performed in triplicate. Data were analyzed using an in-house analysis package[52]. Time course deuterium incorporation levels were generated using an MEM fitting method[53].

Enzymatic assays

KRS was pre-incubated with YH16899 (0 to 40 μM, final concentration) for 30 min at 4°C prior to the reaction, and aminoacylation was performed as described previously[15]. Reaction aliquots were quenched and precipitated in 96-well Multiscreen filter plates (Millipore) as described previously[54]. After washing and elution with 0.2 M NaOH, the samples were quantified on a MicroBeta plate reader (PerkinElmer).

Quantification of the KRS–AIMP2 interaction

A fusion protein of human $AIMP2_{1–48}$ with TRX (thioredoxin) was constructed as described previously[24]. The purified protein was then labeled with EZ-Link-NHS-PEG_{12}-Biotin according to the vendor's instructions (Thermo Scientific). Gradient compound YH16899 and the His-tagged KRS were incubated overnight at 4°C. After adding 0.01 mg/ml (final concentration) of donor beads from the AlphaScreen® Histidine (Nickel Chelate) Detection Kit (PerkinElmer) to the system to incubate for 15 min, 0.01 mg/ml (final concentration) acceptor beads and $AIMP2_{1–48}$-TRX-Biotin were then added to the system and incubated for 1.5 h before quantification on an Envision Plate Reader (Perkin Elmer). This energy is instantly transferred to fluorophores that have long emission half-lives within the same acceptor bead, resulting in emitted light at 520–620 nm. The reactions were carried out at room temperature in white 384-well plates with a total volume of 20 μl. The effect of YH16899 was tested in triplicate with the gradient final concentration of 0–100 μM.

Pharmacokinetics analysis

Compounds (3 mg/kg) were administered intravenously as a solution in 40% dimethylformamide and administered orally as a suspension in 0.5% MC to male ICR mice (n = 4 for each group). After the oral or intravenous administration, blood samples (approximately 50 μl) were collected from an orbital vein at 0.083 (intravenous only), 0.25, 0.5, 1, 2, 4, 8, and 24 h, and the resulting plasma samples were stored in a freezer at −70°C

prior to analysis. After protein precipitation, BC-K01 and YH16899 in plasma were analyzed using an LC/MS/MS system.

Statistical analysis

Student's *t*-test was used for the analysis of differences between groups (SPSS software).

Supplementary Material

Refer to Web version on PubMed Central for supplementary material.

Acknowledgments

This work was supported by the Global Frontier Project grants (NRF-M1AXA002-2010-0029785 [S.K.], NRF-M1AXA002-2010-0029765 [Y.H.J.], NRF-2012M3A6A4054271 [J.W.L.], NRF-2012-054237 [B.W.H.]); by the WCU grant (R31-2008-000-10086-0[G.H.]); by Proteogenomic Research Program (2012M3A9B9036679 [C.L.]) and by ROA-2012-0006262 (A.M.) of NRF funded by the MEST of Korea. This study was also funded by Ministry for Health & Welfare Affairs of Korea through Korea Healthcare technology R&D Project (A092255 [D.-H.N.]) and by a grant from Gyeonggi Research Development Program [S.K.]. This work was supported in part by grants from NIH (GM100136 [M.G.]); by NSF Division of Materials Research through DMR-11-57490 (A.G. Marshall, Florida State University); by the state of Florida (M.G.) and by a Kimmel Scholar Award for Cancer Research (M.G.). We appreciate A.G. Marshall for the support of HDX-MS program and facility, M.-S. Seok (Korea University) for the preparation of nanodisc and Soon W. Lee (Sungkyunkwan University) for X-ray analysis, respectively.

References

1. Steeg PS. Tumor metastasis: mechanistic insights and clinical challenges. Nat Med. 2006; 12:895–904. [PubMed: 16892035]
2. Berno V, et al. The 67 kDa laminin receptor increases tumor aggressiveness by remodeling laminin-1. Endocr Relat Cancer. 2005; 12:393–406. [PubMed: 15947111]
3. Givant-Horwitz V, Davidson B, Reich R. Laminin-induced signaling in tumor cells. Cancer Lett. 2005; 223:1–10. [PubMed: 15890231]
4. Kim DG, et al. Interaction of two translational components, lysyl-tRNA synthetase and p40/37LRP, in plasma membrane promotes laminin-dependent cell migration. FASEB J. 2012; 26:4142–4159. [PubMed: 22751010]
5. Scheiman J, Tseng JC, Zheng Y, Meruelo D. Multiple functions of the 37/67-kd laminin receptor make it a suitable target for novel cancer gene therapy. Mol Ther. 2010; 18:63–74. [PubMed: 19724263]
6. van den Brule FA, et al. Expression of the 67-kD laminin receptor, galectin-1, and galectin-3 in advanced human uterine adenocarcinoma. Hum Pathol. 1996; 27:1185–1191. [PubMed: 8912829]
7. Sanjuan X, et al. Overexpression of the 67-kD laminin receptor correlates with tumour progression in human colorectal carcinoma. J Pathol. 1996; 179:376–380. [PubMed: 8869283]
8. Martignone S, et al. Prognostic significance of the 67-kilodalton laminin receptor expression in human breast carcinomas. J Natl Cancer Inst. 1993; 85:398–402. [PubMed: 8433393]
9. Fontanini G, et al. 67-Kilodalton laminin receptor expression correlates with worse prognostic indicators in non-small cell lung carcinomas. Clin Cancer Res. 1997; 3:227–231. [PubMed: 9815677]
10. Li D, et al. 67-kDa laminin receptor in human bile duct carcinoma. Eur Surg Res. 2009; 42:168–173. [PubMed: 19182490]
11. Batissoco AC, Auricchio MT, Kimura L, Tabith-Junior A, Mingroni-Netto RC. A novel missense mutation p.L76P in the GJB2 gene causing nonsyndromic recessive deafness in a Brazilian family. Braz J Med Biol Res. 2009; 42:168–171. [PubMed: 19274344]
12. Morris GM, et al. AutoDock4 and AutoDockTools4: Automated docking with selective receptor flexibility. J Comput Chem. 2009; 30:2785–2791. [PubMed: 19399780]

13. Allen B Jr. Is CMS's requirement for age-specific clinical evidence before considering coverage for CT colonography reasonable and necessary? J Am Coll Radiol. 2009; 6:606–608. [PubMed: 19720352]
14. Guo M, Ignatov M, Musier-Forsyth K, Schimmel P, Yang XL. Crystal structure of tetrameric form of human lysyl-tRNA synthetase: Implications for multisynthetase complex formation. Proc Natl Acad Sci USA. 2008; 105:2331–2336. [PubMed: 18272479]
15. Ofir-Birin Y, et al. Structural Switch of Lysyl-tRNA Synthetase between Translation and Transcription. Mol Cell. 2013; 49:30–42. [PubMed: 23159739]
16. Park SG, et al. Human lysyl-tRNA synthetase is secreted to trigger proinflammatory response. Proc Natl Acad Sci USA. 2005; 102:6356–6361. [PubMed: 15851690]
17. Kim JY, et al. p38 is essential for the assembly and stability of macromolecular tRNA synthetase complex: implications for its physiological significance. Proc Natl Acad Sci USA. 2002; 99:7912–7916. [PubMed: 12060739]
18. Kwon NH, et al. Dual role of methionyl-tRNA synthetase in the regulation of translation and tumor suppressor activity of aminoacyl-tRNA synthetase-interacting multifunctional protein-3. Proc Natl Acad Sci USA. 2011; 108:19635–19640. [PubMed: 22106287]
19. Nam JS, et al. Transforming growth factor beta subverts the immune system into directly promoting tumor growth through interleukin-17. Cancer Res. 2008; 68:3915–3923. [PubMed: 18483277]
20. Sevenich L, et al. Transgenic expression of human cathepsin B promotes progression and metastasis of polyoma-middle-T-induced breast cancer in mice. Oncogene. 2011; 30:54–64. [PubMed: 20818432]
21. Arguello F, et al. Incidence and distribution of experimental metastases in mutant mice with defective organ microenvironments (genotypes Sl/Sld and W/Wv). Cancer Res. 1992; 52:2304–2309. [PubMed: 1559233]
22. Perot S, Sperandio O, Miteva MA, Camproux AC, Villoutreix BO. Druggable pockets and binding site centric chemical space: a paradigm shift in drug discovery. Drug Discov Today. 2010; 15:656–667. [PubMed: 20685398]
23. Cheng AC, et al. Structure-based maximal affinity model predicts small-molecule druggability. Nat Biotechnol. 2007; 25:71–75. [PubMed: 17211405]
24. Fang P, et al. Structural context for mobilization of a human tRNA synthetase from its cytoplasmic complex. Proc Natl Acad Sci USA. 2011; 108:8239–8244. [PubMed: 21536907]
25. Omar A, Reusch U, Knackmuss S, Little M, Weiss SF. Anti-LRP/LR-specific antibody IgG1-iS18 significantly reduces adhesion and invasion of metastatic lung, cervix, colon and prostate cancer cells. J Mol Biol. 2012; 419:102–109. [PubMed: 22391421]
26. Zuber C, et al. Invasion of tumorigenic HT1080 cells is impeded by blocking or downregulating the 37-kDa/67-kDa laminin receptor. J Mol Biol. 2008; 378:530–539. [PubMed: 18387633]
27. Lukk M, et al. A global map of human gene expression. Nat Biotechnol. 2010; 28:322–324. [PubMed: 20379172]
28. Hippo Y, et al. Global gene expression analysis of gastric cancer by oligonucleotide microarrays. Cancer Res. 2002; 62:233–240. [PubMed: 11782383]
29. Hura GL, et al. Robust, high-throughput solution structural analyses by small angle X-ray scattering (SAXS). Nat Methods. 2009; 6:606–612. [PubMed: 19620974]
30. Young IS, Nicholls DP. Lipid metabolism. Curr Opin Lipidol. 2010; 21:550–551. [PubMed: 21206344]
31. Pettersen EF, et al. UCSF Chimera--a visualization system for exploratory research and analysis. J Comput Chem. 2004; 25:1605–1612. [PubMed: 15264254]
32. Soares MR, de Paula FO, Chaves M, Assis NM, Chaves Filho HD. Patient with Down syndrome and implant therapy: a case report. Braz Dent J. 2010; 21:550–554. [PubMed: 21271047]
33. Schmidlin K, et al. Complication and failure rates in patients treated for chronic periodontitis and restored with single crowns on teeth and/or implants. Clin Oral Implants Res. 2010; 21:550–557. [PubMed: 20443806]
34. Otani A, et al. A fragment of human TrpRS as a potent antagonist of ocular angiogenesis. Proc Natl Acad Sci USA. 2002; 99:178–183. [PubMed: 11773625]

35. Cardin V, Friston KJ, Zeki S. Top-down modulations in the visual form pathway revealed with dynamic causal modeling. Cereb Cortex. 2011; 21:550–562. [PubMed: 20621984]
36. Ford CL, Randal-Whitis L, Ellis SR. Yeast proteins related to the p40/laminin receptor precursor are required for 20S ribosomal RNA processing and the maturation of 40S ribosomal subunits. Cancer Res. 1999; 59:704–710. [PubMed: 9973221]
37. Kawamata H, Magrane J, Kunst C, King MP, Manfredi G. Lysyl-tRNA synthetase is a target for mutant SOD1 toxicity in mitochondria. J Biol Chem. 2008; 283:28321–28328. [PubMed: 18715867]
38. Kim ES, et al. Sphingosine 1-phosphate regulates matrix metalloproteinase-9 expression and breast cell invasion through S1P3-Galphaq coupling. J Cell Sci. 2011; 124:2220–2230. [PubMed: 21652634]
39. Nyberg P, et al. Endostatin inhibits human tongue carcinoma cell invasion and intravasation and blocks the activation of matrix metalloprotease-2, -9, and -13. J Biol Chem. 2003; 278:22404–22411. [PubMed: 12690120]
40. Shenkarev ZO, et al. Lipid-protein nanodiscs: possible application in high-resolution NMR investigations of membrane proteins and membrane-active peptides. Biochemistry (Mosc). 2009; 74:756–765. [PubMed: 19747096]
41. Delaglio F, et al. NMRPipe: a multidimensional spectral processing system based on UNIX pipes. J Biomol NMR. 1995; 6:277–293. [PubMed: 8520220]
42. Vranken WF, et al. The CCPN data model for NMR spectroscopy: development of a software pipeline. Proteins. 2005; 59:687–696. [PubMed: 15815974]
43. Kim KA, et al. Structure of human PRL-3, the phosphatase associated with cancer metastasis. FEBS Lett. 2004; 565:181–187. [PubMed: 15135076]
44. Putnam CD, Hammel M, Hura GL, Tainer JA. X-ray solution scattering (SAXS) combined with crystallography and computation: defining accurate macromolecular structures, conformations and assemblies in solution. Q Rev Biophys. 2007; 40:191–285. [PubMed: 18078545]
45. Konarev PV, Volkov VV, Sokolova AV, Koch MHJ, Svergun DI. PRIMUS: a Windows PC-based system for small-angle scattering data analysis. J Appl Crystal. 2003; 36:1277–1282.
46. Svergun DI. Determination of the regularization parameter in indirect-transform methods using perceptual criteria. J Appl Cryst. 1992; 25:495–513.
47. Franke D, Svergun DI. DAMMIF, a program for rapid ab-initio shape determination in small-angle scattering. J Appl Cryst. 2009; 42:342–346.
48. Zhang HM, et al. Enhanced digestion efficiency, peptide ionization efficiency, and sequence resolution for protein hydrogen/deuterium exchange monitored by Fourier transform ion cyclotron resonance mass spectrometry. Anal Chem. 2008; 80:9034–9041. [PubMed: 19551977]
49. Zhang HM, Bou-Assaf GM, Emmett MR, Marshall AG. Fast reversed-phase liquid chromatography to reduce back exchange and increase throughput in H/D exchange monitored by FT-ICR mass spectrometry. J Am Soc Mass Spectrom. 2009; 20:520–524. [PubMed: 19095461]
50. Zhang HM, et al. Simultaneous reduction and digestion of proteins with disulfide bonds for hydrogen/deuterium exchange monitored by mass spectrometry. Anal Chem. 2010; 82:1450–1454. [PubMed: 20099838]
51. Schaub TM, et al. High-performance mass spectrometry: Fourier transform ion cyclotron resonance at 14.5 Tesla. Anal Chem. 2008; 80:3985–3990. [PubMed: 18465882]
52. Kazazic S, et al. Automated data reduction for hydrogen/deuterium exchange experiments, enabled by high-resolution Fourier transform ion cyclotron resonance mass spectrometry. J Am Soc Mass Spectrom. 2010; 21:550–558. [PubMed: 20116280]
53. Zhang Z, Li W, Logan TM, Li M, Marshall AG. Human recombinant [C22A] FK506-binding protein amide hydrogen exchange rates from mass spectrometry match and extend those from NMR. Protein Sci. 1997; 6:2203–2217. [PubMed: 9336843]
54. Beebe K, Waas W, Druzina Z, Guo M, Schimmel P. A universal plate format for increased throughput of assays that monitor multiple aminoacyl transfer RNA synthetase activities. Anal Biochem. 2007; 368:111–121. [PubMed: 17603003]

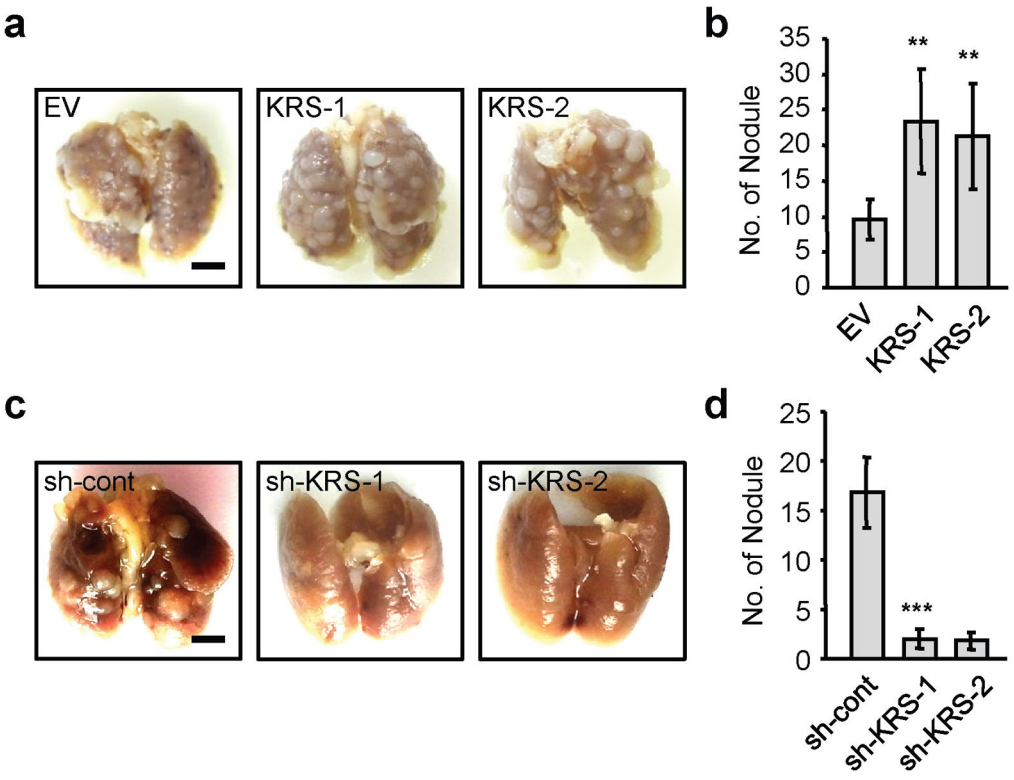

Figure 1. Eeffects of KRS on cancer metastasis

(**a–d**) Established stable mouse breast carcinoma 4T1 cells with high expression of KRS (KRS-1 and KRS-2) or low expression of KRS (sh-KRS-1 and sh-KRS-2) were injected subcutaneously on the back of BALB/cAnCr mice (*n* = 5). After we sacrificed the mice, we assessed cancer metastasis by pulmonary nodule formation (scale bar = 0.5 cm) (**a**, **c**). The numbers of pulmonary nodules (>1 mm in size) of stable KRS-1/2 cells (**b**) and stable sh-KRS-1/2 cells (**d**) were counted and presented as mean ± s.d. (**b:** ** $P < 0.01$; **d:** *** $P < 0.001$).

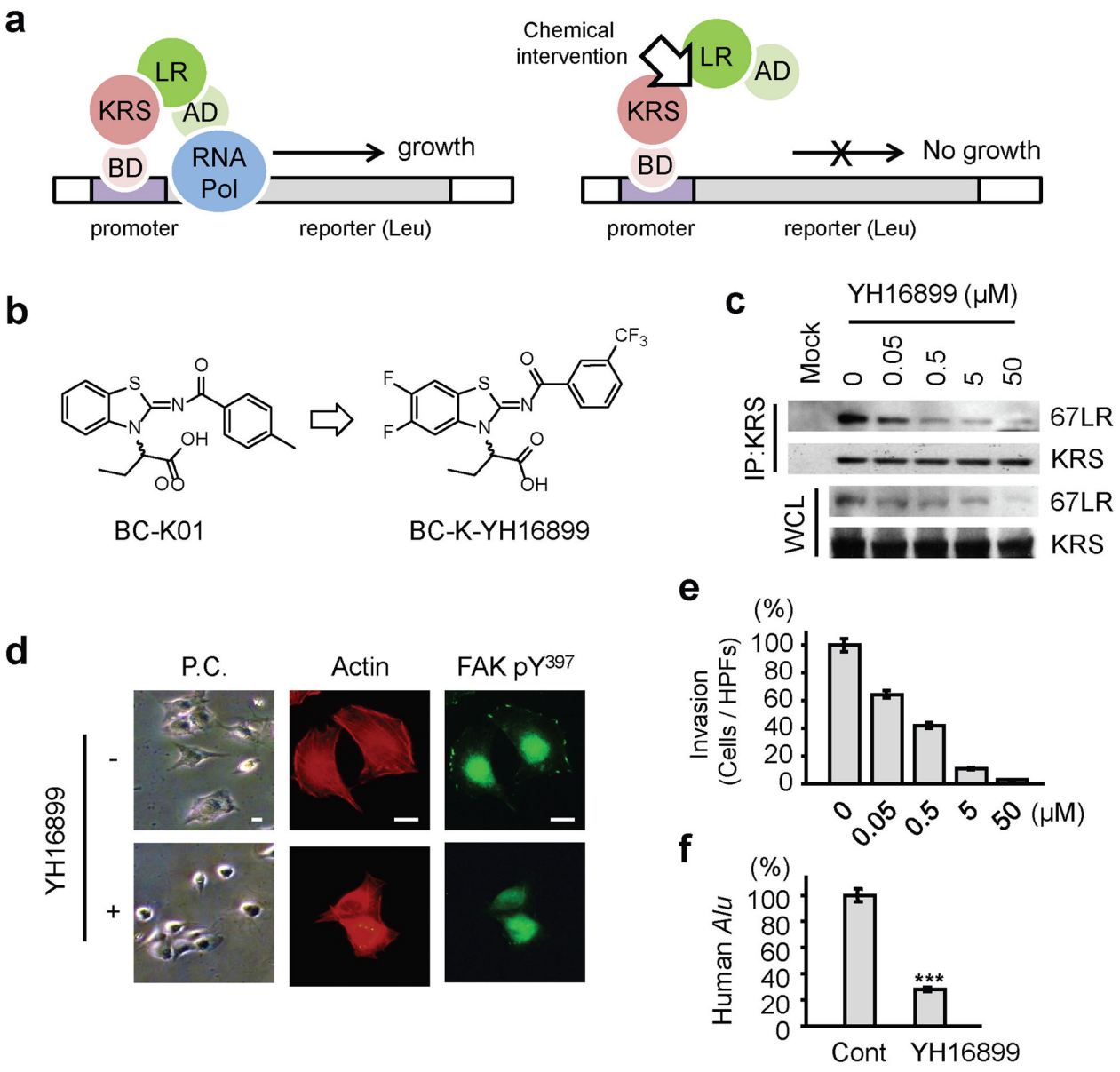

Figure 2. Identification of YH16899 inhibiting KRS–LR interaction and cell invasion

(**a**) A schematic diagram of the screening strategy for an Y2H assay. KRS and 37LRP were fused to a DNA-binding domain (BD, LexA) and an activating domain (AD, B42) of a transcription factor, respectively. Yeast cells co-expressing these fusion proteins survive because BD and AD are brought in proximity via the KRS–LR interaction initiating transcription of a reporter gene (left). If chemicals interfere with the KRS–LR interaction, transcription of the reporter gene cannot occur and yeast cells cannot grow (right). (**b**) Chemical structure of the initial compound BC-K01 and its derivative YH16899. (**c**) H226 cells were incubated with YH16899, and KRS was immunoprecipitated for the detection of coprecipitated 67LR level using immunoblotting; WCL, whole cell lysate (See Supplementary Fig. 24 for raw data). (**d**) KRS-transfected H226 cells were treated with YH16899 (50 μM). Cell morphology was monitored using phase contrast (P.C.) microscopy

(left). Actin and FAK activity were determined using immunofluorescence staining with rhodamine phalloidin (red, middle) and anti–phospho-Y397 (pY^{397})-FAK antibody (green, right), respectively (scale bar = 10 μm). (**e**) H226 cells were subjected to a Matrigel invasion assay in the presence of YH16899, and the number of cells penetrating the membrane were counted and presented as mean ± s.d. (**f**) H226 cells and YH16899 (50 μM) mixture were injected into the upper layer of CAM and incubated to promote invasion. The amount of human *Alu* gene was presented as mean ± s.d. ($n = 3$; *** $P < 0.001$).

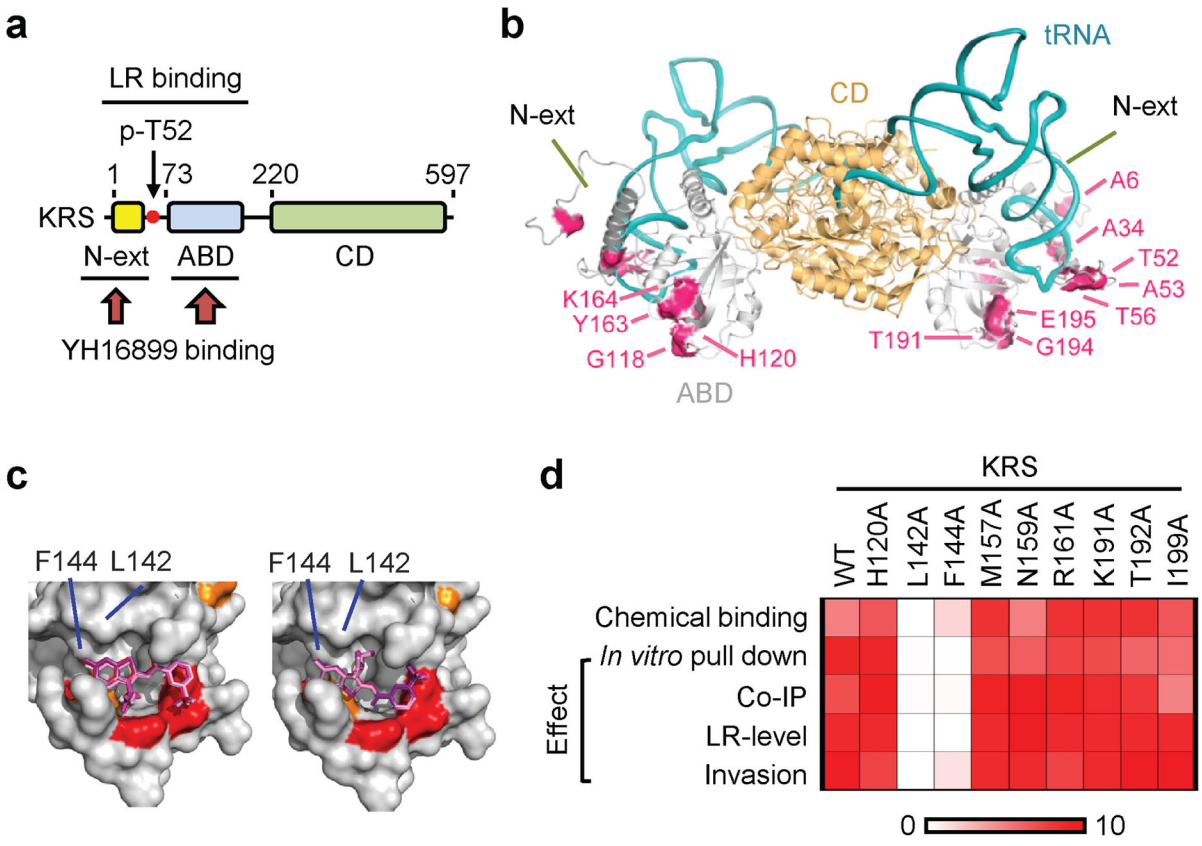

Figure 3. Mapping and validation of an YH16899 docking site

(**a**) A schematic of the functional domain arrangement in human KRS. KRS contains an N-terminal extension domain (N-ext), an anticodon-binding domain (ABD), and a catalytic domain (CD). The T52 residue (undergoes phosphorylation) is indicated as a red dot. N-ext and ABD of KRS specifically interact with LR and YH16899. Arrow width indicates intensity of the compound–KRS interaction. (**b**) Spatial arrangement of the chemically perturbed residues (red) on KRS with $tRNA^{Lys}$. (**c**) Docking positions of the *R*- (left) and *S*- (right) YH16899 in the hydrophobic pocket of KRS were identified in NMR experiments. Ten low-energy positions were represented, and the CSP-defined residues are shown in red. (**d**) A summary of the critical residues around the YH16899 binding site. Specific residues were replaced with alanine, and the effects of the mutations on the binding to YH16899 and LR (*in vitro* pull-down and co-IP), 67LR stability, and cell invasion were examined (see Supplementary Fig. 18). The results of these experiments were calculated based on the relative band intensities (pull-down, IP, and 67LR level) and the relative numbers of migratory cells (invasion assay), and presented as a heat map with the scale from 0 to 10. For the SPR, a –log-transformed value of each K_D was obtained and presented on a scale from 0 (K_D, 1×10^{-3}) to 10 (K_D, 1×10^{-10}). The location of L142 and F144 in ABD, the most critical residues, is denoted in Fig. 3c.

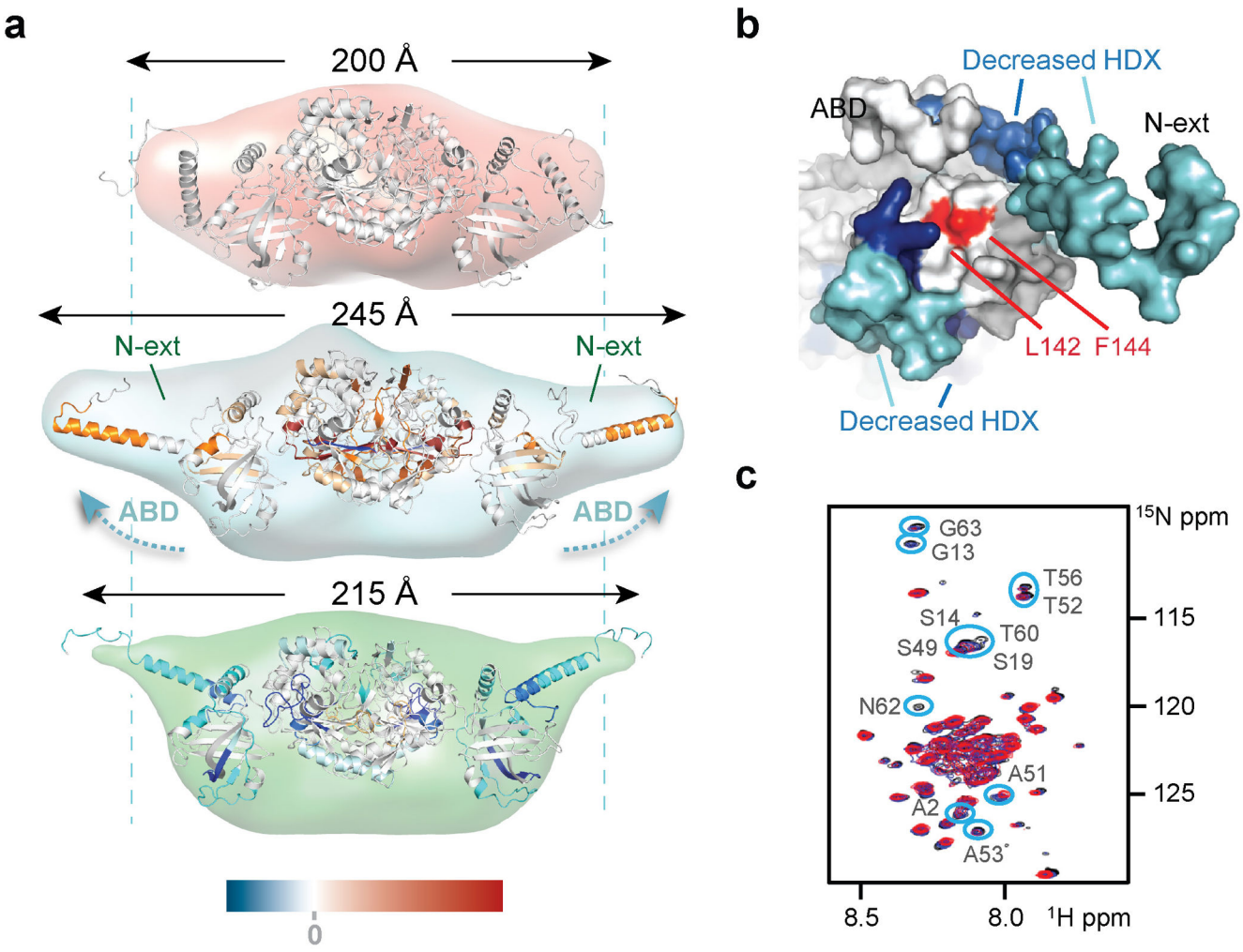

Figure 4. Effects of YH16899 binding on the KRS structure

(**a**) SAXS and HDX-MS analysis of the effect of YH16899 on conformational changes of dimeric KRS T52D. KRS T52D has a more extended N-terminus and open ABD-CD interface compared to WT KRS, partially exposing the AIMP2-binding site. Incubation of KRS T52D with YH16899 induced a conformational change folding N-ext back toward the body of KRS. Blue and red indicate a less and more exposed surface, respectively. KRS WT was used as a control. (**b**) HDX-MS analysis of the effect of YH16899 on conformational changes of KRS T52D. Fragments of both N-ext and ABD showed decreased deuterium uptake in T52D + YH16899 compared to T52D alone. Cyan, 20%–40% decrease; Blue, >40% decrease. The mutagenesis-mapped binding site of inhibitor is colored in red. (**c**) CSP of [^{15}N]KRS$_{1–72}$ by means of phospholipid nanodisc binding. Superposition of the 2D ^{1}H-^{15}N TROSY spectra of free 0.2 mM KRS$_{1–72}$ with 0 mM (black), 0.1 mM (blue), and 0.2 mM (red) of the nanodisc. Strongly perturbed residues are denoted as blue circles.

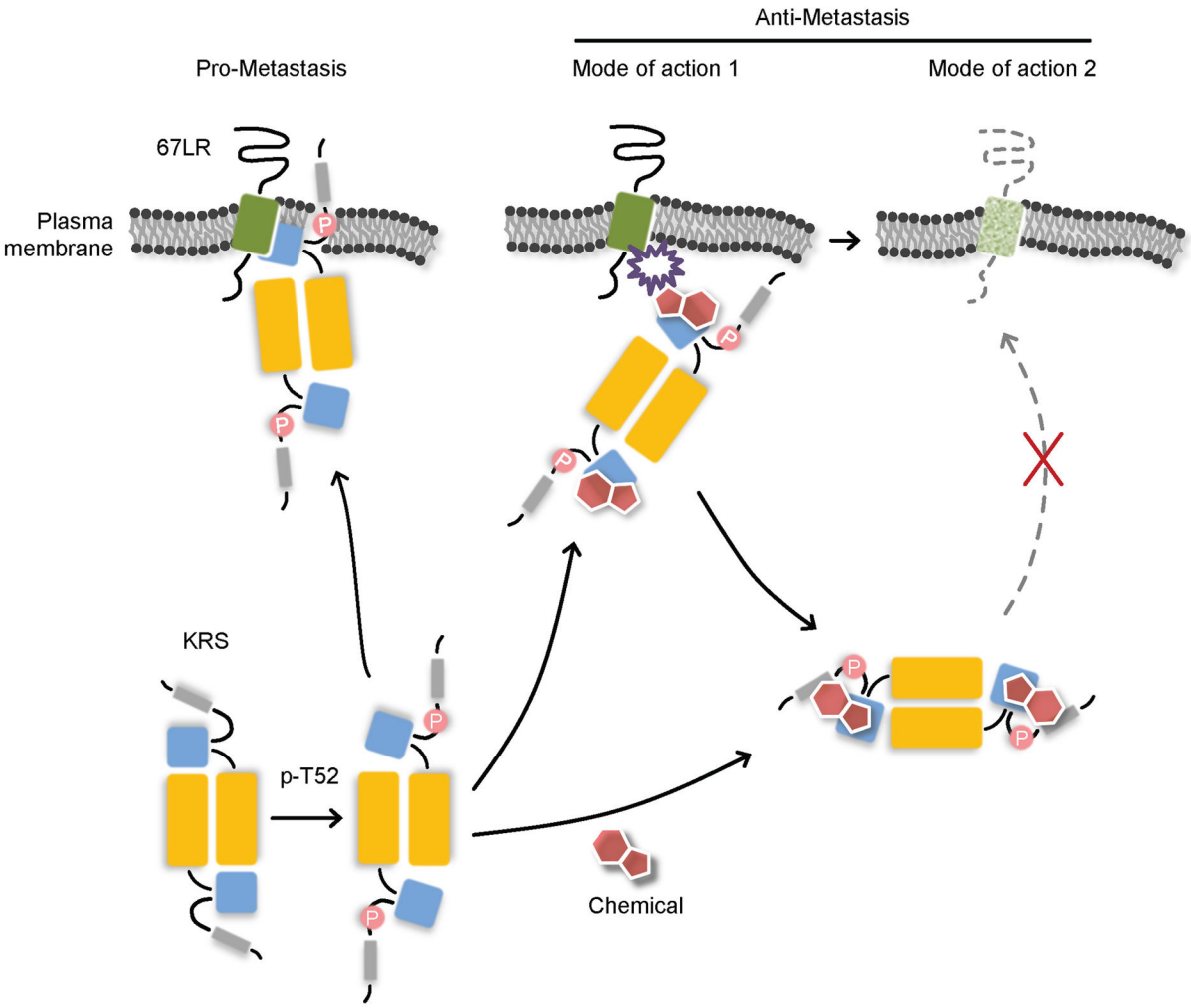

Figure 5. A schematic model for the mode of action of YH16899

Phosphorylation of KRS at T52 induces a conformational change that opens up the AIMP2-binding interface, releasing KRS from MSC. YH16899 binds to KRS ABD (blue) and N-ext (grey) thereby directly inhibiting the interaction between KRS and 67LR. In addition, YH16899's binding to KRS reduces the flexibility of N-ext and reduces the membrane localization of KRS. 67LR in the membrane without binding to KRS undergoes ubiquitin-mediated degradation. Although 67LR is thought to be a dimer of 37LRP, only a monomer is shown for the sake of simplicity.